THE JOURNAL OF PHYSICAL CHEMISTRY LETTERS
A JOURNAL OF THE AMERICAN CHEMICAL SOCIETY

pubs.acs.org/JPCL

Letter

Effects of High and Low Salt Concentrations in Electrolytes at Lithium−Metal Anode Surfaces Using DFT-ReaxFF Hybrid Molecular Dynamics Method

Yue Liu, Qintao Sun, Peiping Yu, Yu Wu, Liang Xu, Hao Yang, Miao Xie, Tao Cheng,* and William A. Goddard III

Cite This: *J. Phys. Chem. Lett.* 2021, 12, 2922−2929

Read Online

ACCESS | Metrics & More | Article Recommendations | Supporting Information

ABSTRACT: Due to creating a passivated solid electrolyte interphase (SEI), high concentration (HC) electrolytes demonstrate peculiar physicochemical properties and outstanding electrochemical performance. However, the structures of such SEI remains far from clear. In this work, a **h**ybrid ***ab initio*** and **r**eactive molecular dynamics (HAIR) scheme is employed to investigate the concentration effect of SEI formation by simulating the reductive degradation reactions of lithium bis(fluorosulfonyl)imide (LiFSI) in 1,3 dioxalane (DOL) electrolytes at concentrations of 1 M, 4 M, and 10 M. The efficient HAIR scheme allows the simulations to reach 1 ns to predict electrolytes' deep products at different concentrations. The simulation findings show that the most critical distinction between HC and its low concentration (LC) analogue is that anion decomposition in HC is much more incomplete when only S−F breaking is observed. These insights are important for the future development of advanced electrolytes by rational design of electrolytes.

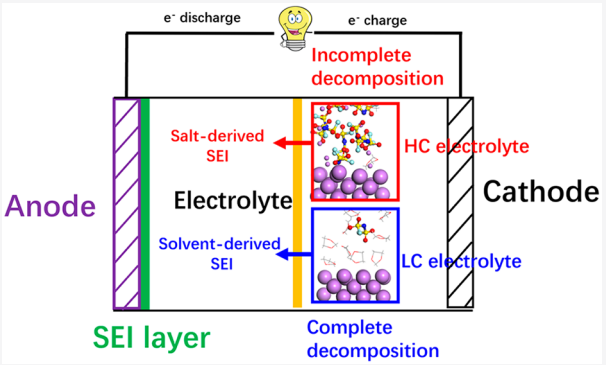

Lithium (Li)-ion batteries (LIBs), serving as a promising candidate to replace conventional energy storage devices, have achieved commercialization in many fields, such as mobile phones, computers, and electric vehicles.[1−3] However, owing to graphite-anode coupled Li^+ interaction/deinteraction cathode used in LIBs, the specific capacity of LIBs is approaching the theoretical values (372m Ah g^{-1}), but it is far from meeting the growing demands for high-energy storage.[4,5] High-voltage (>4.0 V) lithium (Li) metal batteries (LMBs), when using the ideal anode material, Li metal, as the anode, have drawn significant attention owing to its ultrahigh theoretical specific capacity of 3860 m Ah g^{-1} and an extremely low electrochemical potential (−3.040 V vs standard hydrogen electrode, SHE).[6−8] Unfortunately, the high reactivity of Li metal poses a great challenge to the realistic application of LMBs due to the continuous reduction of the solvents and Li-salts in the electrolyte with electrodes during the process of charge and discharge.[9,10] Furthermore, the inevitable dendrite growth of Li and electrolyte reduction by Li metal leads to low Coulombic efficiencies (CEs) and severe safety concerns.[11,12] These important barriers to LMBs are therefore desperately required to build the next generation of high-energy storage equipment.

It is widely accepted that the formation of a solid electrolyte interphase (SEI) plays an important role in determining the stability and performance of Li metal.[13,14] Extensive research has been conducted to investigate and develop SEI in LMBs.[15−18] Strategies are proposed to control the SEI forming process, including the optimization of electrolyte composition,[19,20] the creation of solid electrolytes,[21] and the construction of an artificial SEI sheet.[22,23] For example, high concentration (HC) electrolytes with Li-salts have been developed in recent years to inhibit dendrite growth and enhance CEs.[24] An HC electrolyte system using 7 M lithium bis(trifluoromethane sulfonyl)imide (LiTFSI) concentration dissolved in the mixture of dimethoxyethane (DME) and dioxalane (DOL) in Li/S batteries was suggested by Suo,[25] showing that the HC electrolyte system would overcome two key technological problems at the same time with the polysulfide shuttle and poor lithium metal anode stability. Qian et al.[26] studied the use of salt lithium bis(fluorosulfonyl)-imide (LiFSI) in dimethoxyethane (DME) at high concentrations (up to 4 M) and found that dendrite growth was eliminated, whereas high CEs (>99%) were also achieved. Kim

Received: February 5, 2021
Accepted: March 10, 2021
Published: March 16, 2021

https://doi.org/10.1021/acs.jpclett.1c00279
J. Phys. Chem. Lett. 2021, 12, 2922−2929

et al.[27] conducted experiments by using an ultrahigh LiFSI-based electrolyte resulting in comparable CEs and cycle stability. Theoretically, although many studies on HC electrolyte at the atomic level have been reported, the comprehensive degradation reaction of electrolyte on a Li metal anode with SEI formation is in debate.[28−34] Molecular dynamics (MD) simulations have been known to be one of the most powerful methods for exploring complicated reaction processes by tracking MD trajectories. For example, Camacho-Forero[28] compared the behavior of 1 M and 4 M concentration electrolytes with LiFSI and LiTFSI in DME solvent using the *ab initio* MD (AIMD) process; these theoretical findings indicated that the possible components of the SEI layer depend on the chemical structure of the electrolyte, and LiF was observed as a substance produced by the complete decomposition of LiFSI. In addition, the sacrificial anion reduction process has been explained by Sodeyama and his co-workers,[30] showing that TFSI anions prefer to be reduced by accepting the electron at the high concentration (HC) condition in order to preserve 2 electron reductive solvent decomposition using DFT-MD simulations with explicit solvents and ΔSCF that considers the relaxation of excess electrons after the reductive decomposition of the electrolytes.[30]

Owing to the high computational cost of AIMD, the simulation time scale is limited to dozens of picoseconds (ps), while nanoseconds (ns) to microseconds (ms) are required to clarify the SEI film formation process. Reactive force field (ReaxFF),[35−38] derived from quantum mechanics (QM) results, have been widely used to simulate complex multiphase chemical reactions with much more affordable computational cost. It has been demonstrated that in standard ReaxFF, the lack of explicit consideration of the electron leads to an incorrect description of the electrochemical reaction,[38] which requires more elaborate treatment of the electron in advanced ReaxFF, such as eReaxFF.[39] Thus, a single simulation approach cannot meet the need for long-term MD simulations with reasonable precision and cost.

In this work, a hybrid scheme, hybrid *ab initio* and reactive molecule dynamics (HAIR), that combines AIMD and ReaxFF MD is proposed.[40] The AIMD part of the HAIR method can describe the localized electrochemical reactions accurately, while ReaxFF MD could accelerate chemical reactions and mass transfer with a much more affordable cost while keeping the QM accuracy when the force field parameter is well trained.

To apply the HAIR scheme, we first trained the missing force field parameters of FSI-anions. Relevant ReaxFF parameters are optimized by fitting QM calculations starting from the parameters developed by Islam et al.[38] The optimized ReaxFF parameters and detailed results are shown in the Supporting Information. During the HAIR simulations, the AIMD and ReaxFF simulations are performed with Vienna *Ab Initio* Simulation Package (VASP 5.4.4)[41] and Large-scale Atomic/Molecular Massively Parallel Simulator (LAMMPS 2018)[42] software, respectively. MD simulations are conducted alternatively using the NVT ensemble at 300 K with 1 fs and 0.25 ps timesteps for AIMD and ReaxFF MD simulations while ensuring efficient converge for collisions and smooth reactions. In this work, 10-time acceleration is chosen on liquid electrolyte, in which diffusion is fast, which means that the molecular dynamics simulations start with the AIMD (0.5 ps), followed by ReaxFF MD (5 ps), and continued alternatively.

To describe the electron exchange and correction energies, the Perdew−Burke−Ernzerhof (PBE) functional within the generalized gradient approximation (GGA) is used in this work to conduct AIMD simulation.[43] In addition, we employ the Grimme D3 correction to describe the London dispersion integrations.[44] A 1 × 1 × 1 Monkhorst−Pack[45] k-point mesh was set to sample Brillouin zone integration, and the projector augmented wave (PAW)[46] method as implemented is used to consider electron−ion interactions. As for plane-wave basis expansion, we chose a 400 eV energy cutoff. The threshold for the electronic structure convergence of the self-consistent field was set to 10^{-4} eV with a Gaussian smearing width of 0.2 eV.

Table 1 shows the reaction energies predicted with QM and the ReaxFF method. To prepare the QM training set, the FSI anion is neutralized by adding one H atom. The gas-phase bond dissociation energies with QM results for the S−F and N−S bonds are 83.9 and 54.8 kcal/mol, while the corresponding values are 91.9 and 47.7 kcal/mol with the ReaxFF method. Although the bond energy of S−F is stronger than that of N−S in the gas phase, it is not necessary that the N−S bond must be broken before the S−F bond. As shown in Figure 1a, the S−F bond dissociation curves show that the H atom is bonded with the F atom, indicating that the FSI ion would decompose into the F ion with a reaction energy of 64.4 kcal/mol, which opens the possibility of S−F bond cleavages.

Table 1. Relative Reaction Energies (in kcal/mol) for QM and ReaxFF Method

	relative reaction energies (kcal/mol)	
reaction	QM(B3LYP/6-311+g(d,p))	ReaxFF
$HN(SO_2F)_2$=$HN(SO_2F)SO_2$ + F	83.9	91.9
$HN(SO_2F)_2$=$HNSO_2F$ + SO_2F	54.8	47.7

In order to investigate the initial reaction process to reduce the deterioration of the lithium-electrolyte system, HAIR simulations are performed based on the theoretical model, which contains a Li-slab with a mixed electrolyte of DOL and LiFSI; the detailed information is shown in the Supporting Information. Figure 2 shows the sequence of FSI decomposition during 0−6.0 ps, at approximately 0.5 ps, the Li-FSI-DOL pair is observed in the periodic box through Li−O coordination. The following decomposition stage of the FSI initiates an S−F bond break as expected by QM findings and previous work.[28] After that, the $N(SO_2)_2$ fragment undergoes reductive reaction by Li^0 to form Li_2O, and then the N−S bond is broken into NSO_2 and SO at around 5.6 ps. In order to validate the accuracy of the HAIR simulation, a 3.5 ps long AIMD simulation is performed and more details can be found in the Supporting Information. As shown in Figure 3, the initial reaction of FSI predicted with AIMD is S−F bond cleavage at 1.0 ps, which confirms the HAIR results (1.5 ps). S−F bond breaking is induced by the decomposition process of FSI and preceded by N−S bond cleavage, indicating no variations between DFT-based AIMD and HAIR results.

The purpose of including AIMD is to describe chemical reactions more accurately. Although the training set of ReaxFF is derived from QM calculations, ReaxFF itself cannot fully guarantee the accuracy in describing electrochemical reactions, especially considering that the work function (the electron's chemical potential) significantly changes during the reactions. Therefore, it is still necessary to include the AIMD in the HAIR scheme. Indeed, critical reactions, such as S−F and N−S

https://doi.org/10.1021/acs.jpclett.1c00279
J. Phys. Chem. Lett. 2021, 12, 2922−2929

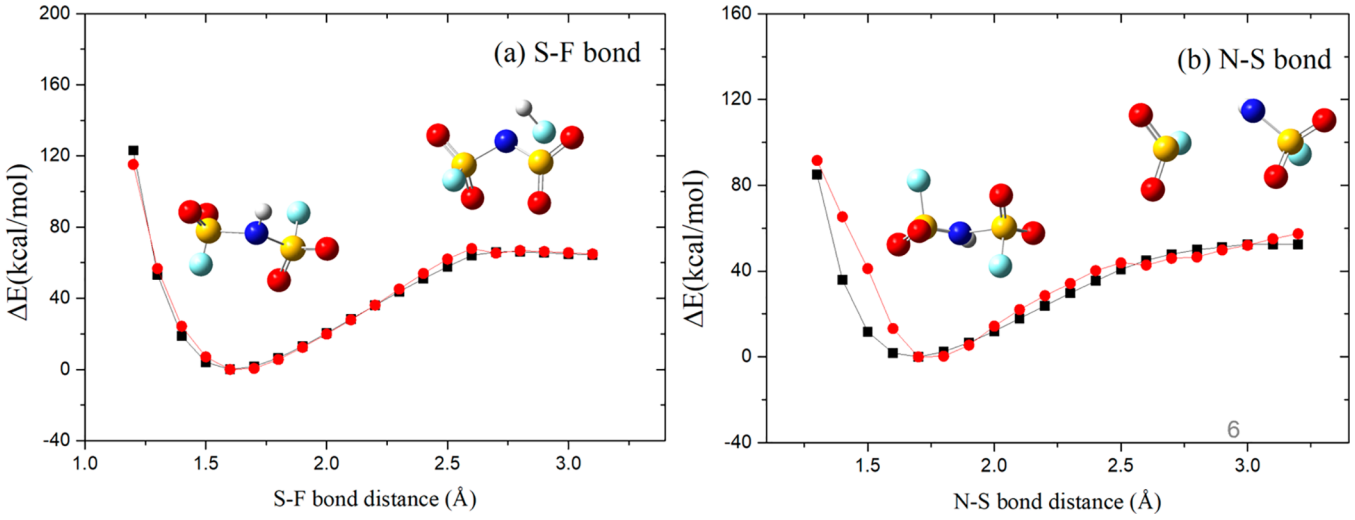

Figure 1. Bond dissociation curves are predicted by QM and the ReaxFF method: (a) S−F bond and (b) N−S bond. The black line is for the QM results, and the red line is for the ReaxFF. The colors are lithium in purple, oxygen in red, carbon in gray, fluorine in cyan, sulfur in yellow, nitrogen in blue, and hydrogen in white.

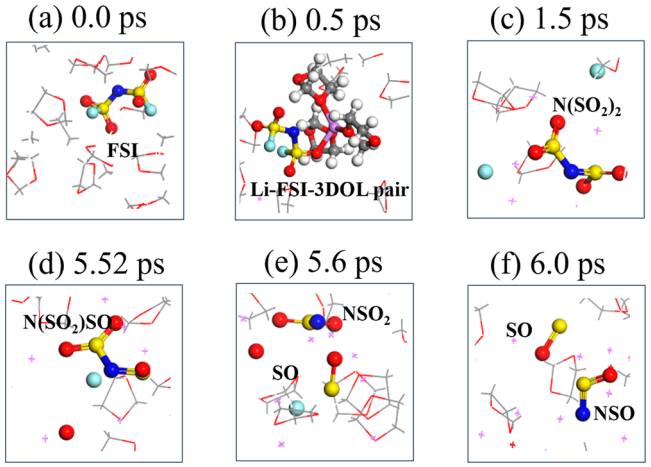

Figure 2. Sequences of FSI decomposition were obtained from HAIR simulations for the DOL/LiFSI mixture between 0 and 6.0 ps: (a) 0.0 ps, (b) 0.5 ps, (c) 1.5 ps, (d) 5.52 ps, (e) 5.6 ps, and (f) 6.0 ps. The colors are lithium in purple, oxygen in red, carbon in gray, fluorine in cyan, sulfur in yellow, nitrogen in blue, and hydrogen in white.

bond cleavages of FSI are observed in the AIMD loop, which is basically in line with our expectations. That is, AIMD guarantees the accuracy of the chemical reactions, while ReaxFF speeds up the mass transfer.

The concentration effect of FSI in SEI formation is investigated by carrying out HAIR simulations at different concentrations of 1 M, 4 M, and 10 M (ultrahigh concentrations in the experiment).[47] Figure 4 shows the snapshots of HAIR simulation at 275 ps of simulations with different concentrations. The simulation results of LC are shown in Figure 4a, which implies the complete decomposition of FSI anion into LiSN, SO, LiF, and Li_2O products. Meanwhile, the reduction reaction of DOL is also observed, which is reduced by Li^0 via ring-opening process to form C_2H_4, LiOCHO, CH_2O, $LiOCH{=}CH_2$. Similar simulation results were also reported by Yun et al.[48] Additionally, the simulation results of a medium concentration (MC, 4 M) are shown in Figure 4b. The major difference between MC and LC is that the decomposition of FSI- is incomplete in MC. At the same time, no DOL decomposition was observed in MC. The difference in initial reactions is more significant when compared with the cases of LC and HC. As shown in Figure 4c, only S−F bond-breaking was observed in HC, while all the backbone of FSI anions still exists in the electrolyte. As expected, no DOL decomposition was observed. With the increase of salt concentration, LiFSI decomposed to consume free Li^0 to prevent DOL from reducing, which has been proposed as the "sacrificial reaction mechanism" by Sodeyama.[30]

In order to further investigate the components and structure of the SEI sheet, the time scale HAIR simulations with various concentrations are expanded to 605 ps, followed by 400 ps ReaxFF MD and 10 ps AIMD simulations. In Figure 5, these snapshots exhibit significant differences at different concentrations after 1 ns simulation. At 1 M and 4 M concentrations, the SEI layer was formed with clusters and cavities, introducing a heterogeneous SEI layer. While a homogeneous and stable layer, consisting of a typical inorganic layer by the order of Li−O, Li−S, and Li−F coordination, is observed at the HC (10 M) concentration. A layer of SEI majoring in Li_xF is observed after 1.015 ns HAIR simulation that consists of 0.055 ns AIMD and 0.96 ns ReaxFF MD. Such Li_xF layer is generally believed to play a crucial role in stabilizing the lithium anode. In the work of Ospina-Acevedo et al., they also reported the formation of a similar Li_xF layer at lower concentration (2 M), larger simulation size (~20 nm^3), and longer time scale (~20 ns).[49]

Figure 6 shows the radial distribution function (RDF) and the integrated number of different bonds after long-time simulations with LC, MC, and HC concentrations. Apparently, similar peaks at around 2 Å are observed for Li−F and Li−O bonds at different concentrations, which implies the stable products LiF and Li_2O are formed during MD simulations to contribute to the inorganic layer of SEI film as mentioned by Ospina-Acevedo.[49] It is a remarkable fact that the Li−F bond RDF shows significant differences for 1 M, 4 M, and 10 M LiFSI systems, and several sharpened peaks are seen between 3 and 8 Å for the 1 M LiFSI system, while smooth curves are shown in MC and HC concentrations (4 and 10 M LiFSI systems). Obviously, in the HC concentrations, free Li^0 are

https://doi.org/10.1021/acs.jpclett.1c00279
J. Phys. Chem. Lett. 2021, 12, 2922−2929

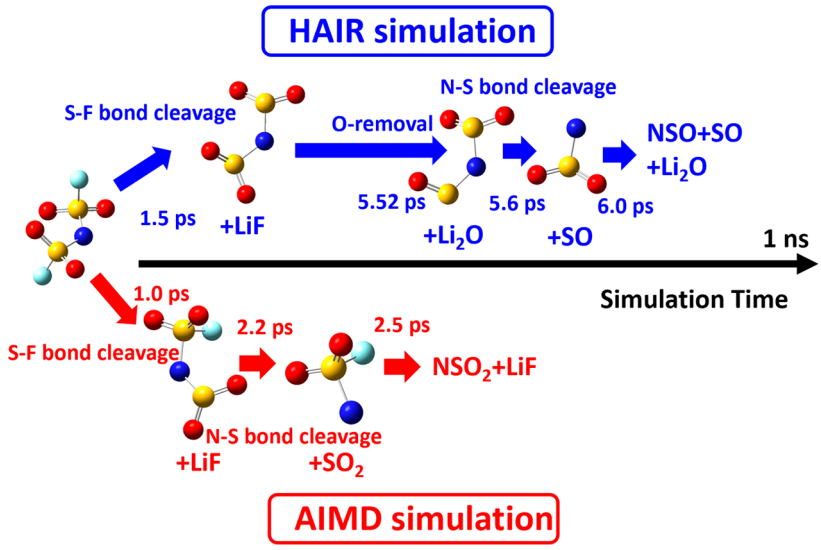

Figure 3. Reaction pathway obtained from HAIR (blue) and AIMD (red) simulations.

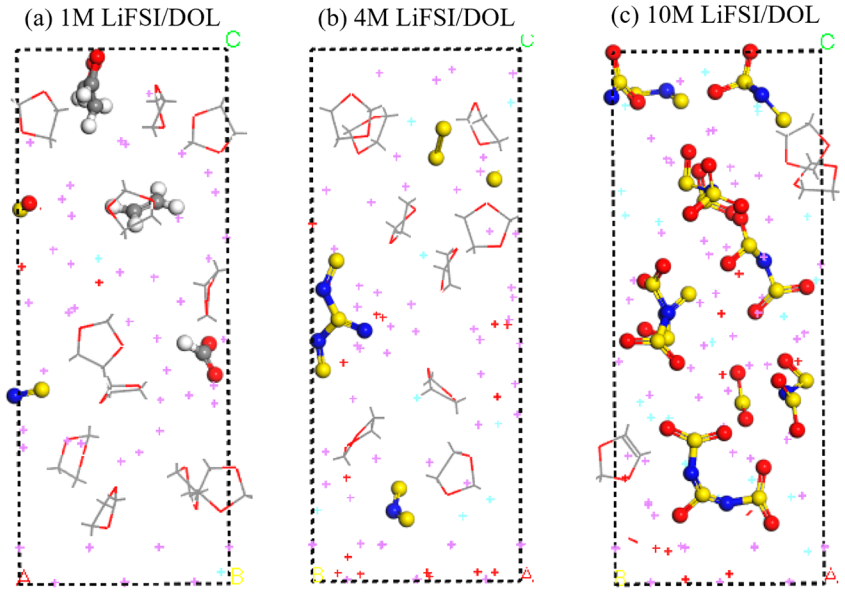

Figure 4. Snapshots from MD simulation at 275 ps for (a) 1 M LiFSI/DOL, (b) 4 M LiFSI/DOL, and (c) 10 M LiFSI/DOL. The colors are lithium in purple, oxygen in red, carbon in gray, fluorine in cyan, sulfur in yellow, nitrogen in blue, and hydrogen in white.

consumed by the decomposition fragments of LiFSI with a large amount of LiF formed, but for the LC system, only serval peaks could be found as the inorganic parts (LiF). According to Figure 6c,d, effects on the decomposition processes of LiFSI with different concentrations are also verified by the RDF analyses for Li−S and S−O bonds, in 1 M and 4 M concentrations, the obvious peaks are found in Li−S RDF at 2.4 Å while no peaks are shown in S−O bond. In contrast to the 1 M and 4 M LiFSI systems, a clear peak is identified at 1.7 Å for the S−O bond. These RDF results indicate that the LiFSI are decomposed incompletely with no Li_2S formed in the 10 M LiFSI/DOL system, showing a good agreement with the snapshots at 275 ps with different concentrations.

To further identify the different components of SEI film at different concentrations, Figure 7 shows the main products obtained from long-time simulations (more than 1 ns), and other products are listed in Table 2. In 1 M LiFSI/DOL electrolyte, the SEI film is comprised of the inorganic layer (LiF, Li_2O, Li_2S) and the organic layer (LiCHO, LiOCH═CH_2, etc.), which mainly derives from the reduction of LiFSI and DOL. Concerning the 4 M LiFSI/DOL system, the SEI film includes inorganic part LiF, Li_2O, Li_2S, and N_2 gas, indicating salt-derived SEI formation as predicted by previous work.[28,30] With regard to the ultrahigh concentrations, more stable products are clarified in SEI inorganic parts, such as Li_2CO_3 and Li_2SO_3, which are identified to be the main parts of the SEI layer as experimentally.[32] Additionally, owing to the incomplete decomposition of TFSI ions, LiF is prior to being generated with the consumption of free Li^0, which are the main compositions of the SEI layer formed at HC electrolyte, while more Li_2O are observed in the MC system. As the increase of concentrations, we also found LiF show a continuous increase, and no Li_2S was seen in the HC system as predicted by RDF analyses.

For the sake of exploring the LiF after 1 ns long simulations, X-ray photoelectron spectroscopy (XPS) is employed. A

https://doi.org/10.1021/acs.jpclett.1c00279
J. Phys. Chem. Lett. 2021, 12, 2922−2929

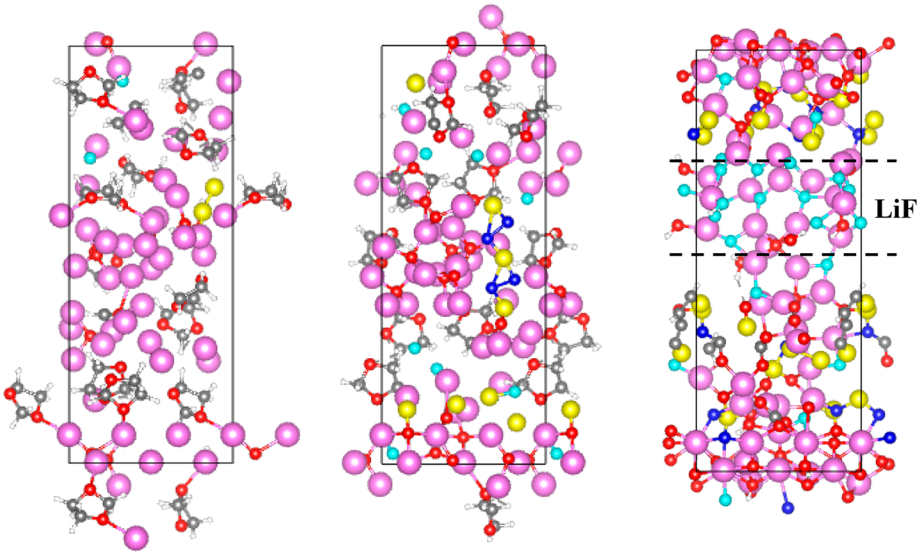

Figure 5. Snapshots from MD simulation after 1 ns for (a) 1 M LiFSI/DOL, (b) 4 M LiFSI/DOL, and (c) 10 M LiFSI/DOL. The colors are lithium in purple, oxygen in red, carbon in gray, fluorine in cyan, sulfur in yellow, nitrogen in blue, and hydrogen in white.

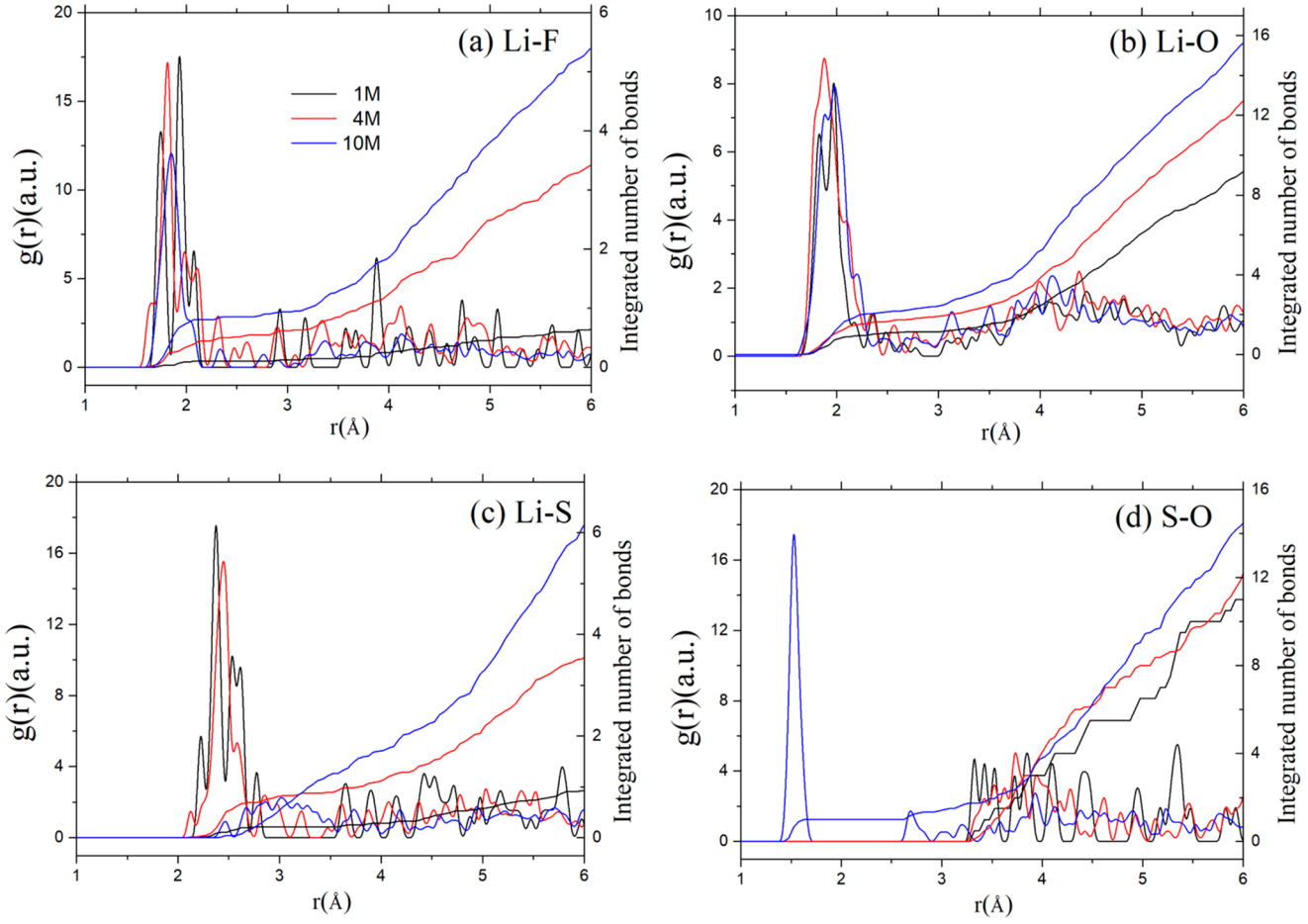

Figure 6. Radial distribution function and integrated number of bonds for (a) Li−F, (b) Li−O, (c) Li−S, and (d) S−O after 605 ps HAIR, 400 ReaxFF, and 10 ps AIMD simulations. The black line is for 1 M LiFSI/DOL; the red line is for 4 M LiFSI/DOL; and the blue line for 10 M LiFSI/DOL.

thousand structures from the last 5 ps AIMD simulations are selected to simulate the XPS spectra, and the binding energies are calculated by initial state approximation using VASP at the PBE-D3 level.[50] Statistical distributions are fitted with the

https://doi.org/10.1021/acs.jpclett.1c00279
J. Phys. Chem. Lett. 2021, 12, 2922−2929

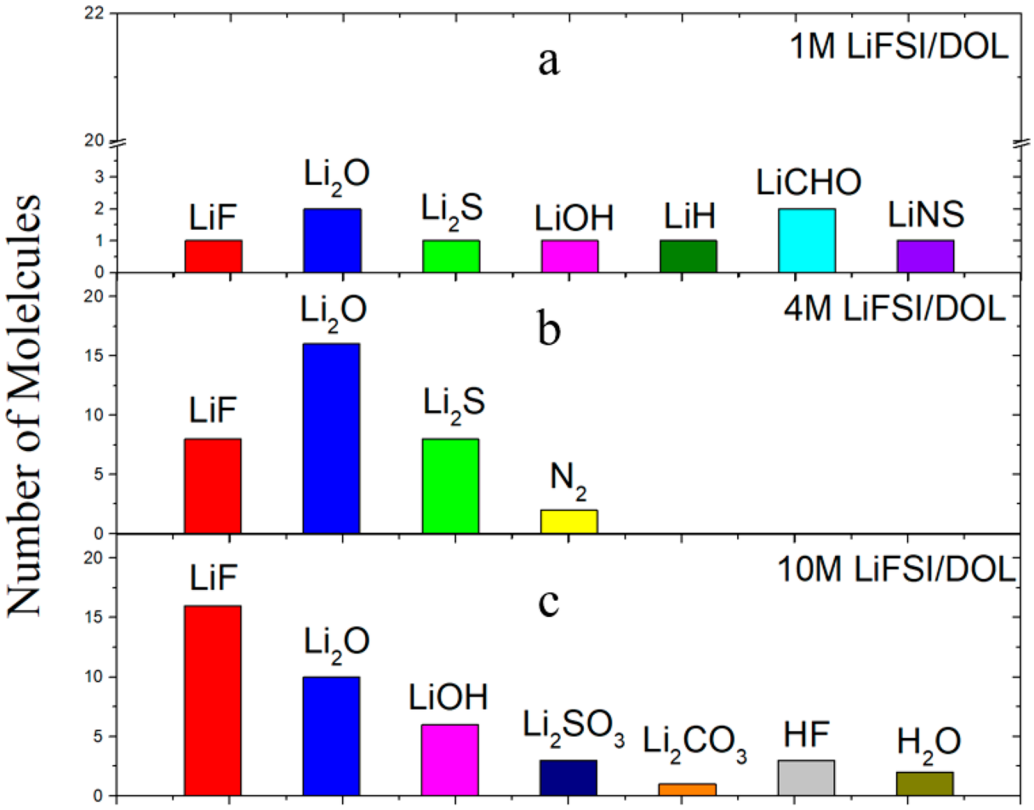

Figure 7. Main product distributions after 1 ns long-time simulations at concentrations of (a) 1 M LiFSI/DOL, (b) 4 M LiFSI/DOL, and (c) 10 M LiFSI/DOL.

Table 2. Products Obtained from HAIR MD Simulation after 1 ns for 1 M LiFSI/DOL, 4 M LiFSI/DOL, and 10 M LiFSI/DOL Systems

	main products
1 M LiFSI/DOL	LiH, LiF, Li_2O, LiOH, Li_2S, LiNS, C_2H_5F, LiCHO, $LiOCH{=}CH_2$
4 M LiFSI/DOL	LiF, Li_2O, Li_2S, N_2
10 M LiFSI/DOL	LiF, Li_2O, LiNSO, LiSF, Li_2CO_3, Li_2SO_3, LiOH, $LiNSO_2$, LiH, HF, H_2O

Gaussian function as shown in Figure 8.[51] The binding energy of S−F, H−F, and Li−F is 657.2 eV, 655.5 eV, and 654.1−654.4 eV, respectively, which indicates binding energy shift of Li−F to S−F is −2.95 ± 0.15 eV, showing a good agreement with binding energy shift −2.9 eV predicted experimentally.[52] In addition, an obvious increase of intensity for LiF is seen along with a concentration increase as the product distribution is predicted.

In summary, a hybrid AIMD-ReaxFF scheme (HAIR) that combines QM and MM reactive dynamics, is employed to investigate the reduction reaction and SEI formation at different concentrations (1 M, 4 M, and 10 M LiFSI/DOL electrolyte systems). To achieve the ReaxFF MD part in HAIR simulations, parameters are developed by training QM-based calculations. The reduction reaction of LiFSI obtained from HAIR simulations is initiated by S−F bond cleavage and followed by N−S bond breaking, which is not only supported by QM calculations but also verified by short AIMD simulations. On the basis of the reliable initial reactions using the HAIR method, MD simulations are extended to 1 ns long to clarify the effects on the degradation reduction of electrolyte and compositions of the SEI layer with different salt

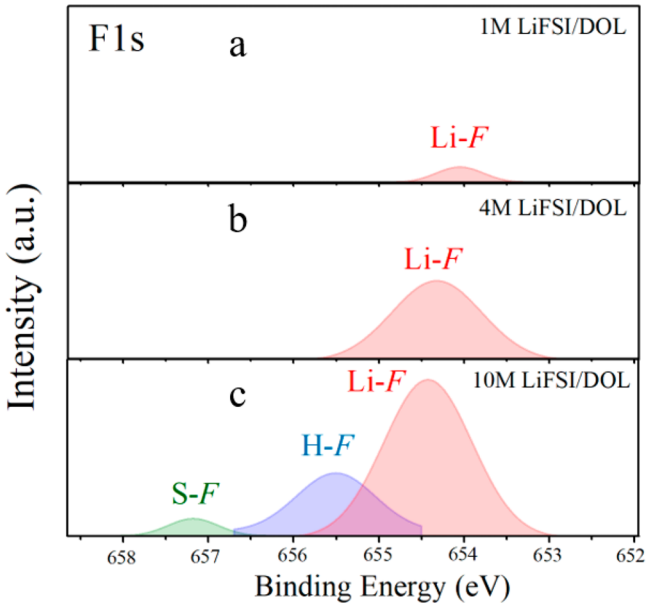

Figure 8. XPS spectra of F_{1s} of (a) 1 M FSI-DOL (b) 4 M FSI-DOL, and (c) 10 M FSI-DOL, respectively.

concentrations, including 1 M, 4 M, and 10 M LiFSI/DOL electrolyte systems. Accordingly, our theoretical results indicate that the complete decomposition of FSI ion and DOL solvent contributes to the inorganic and organic parts of the SEI layer in the LC system. Instead, in HC electrolyte, FSI ions decomposed incompletely via initial S−F bond breaking to consume free Li^0, which prevents the solvent DOL from reducing sacrificially. Further RDF and XPS analysis imply the

https://doi.org/10.1021/acs.jpclett.1c00279
J. Phys. Chem. Lett. 2021, 12, 2922−2929

differences of SEI compositions for LC, MC, and HC electrolytes, as the result of the significant reaction mechanism is affected by salt-concentrations. The main products of the LC system contain LiF, Li_2O, Li_2S, LiCHO, and $LiOCH{=}CH_2$ while more inorganic products, such as Li_2CO_3 and Li_2SO_3, LiF, and Li_2O, are identified in HC electrolyte, and the product distributions show that LiF shows a continuous increase along with the increase of concentration, and Li_2S does not exist in HC systems due to the incomplete decomposition of LiFSI. These theoretical results demonstrate the SEI formation switches from the solvent-derived layer to salt-derived SEI layer by simply increasing salt concentrations, which supply new insights for further developments of advanced electrolytes.

■ ASSOCIATED CONTENT

Supporting Information

The Supporting Information is available free of charge at https://pubs.acs.org/doi/10.1021/acs.jpclett.1c00279.

Details of reactive force field parameters optimization, force field parameters, model of the lithium-electrolyte system, short AIMD results, and XRD patterns from MD simulations for 1 M LiFSI/DOL, 4 M LiFSI/DOL, and 10 M LiFSI/DOL systems after long-time simulations (more than 1 ns) (PDF)

■ AUTHOR INFORMATION

Corresponding Author

Tao Cheng − *Institute of Functional Nano and Soft Materials (FUNSOM), Soochow University, Suzhou 215123, China;* orcid.org/0000-0003-4830-177X; Email: tcheng@suda.edu.cn

Authors

Yue Liu − *Institute of Functional Nano and Soft Materials (FUNSOM), Soochow University, Suzhou 215123, China*

Qintao Sun − *Institute of Functional Nano and Soft Materials (FUNSOM), Soochow University, Suzhou 215123, China*

Peiping Yu − *Institute of Functional Nano and Soft Materials (FUNSOM), Soochow University, Suzhou 215123, China*

Yu Wu − *Institute of Functional Nano and Soft Materials (FUNSOM), Soochow University, Suzhou 215123, China*

Liang Xu − *Institute of Functional Nano and Soft Materials (FUNSOM), Soochow University, Suzhou 215123, China*

Hao Yang − *Institute of Functional Nano and Soft Materials (FUNSOM), Soochow University, Suzhou 215123, China;* orcid.org/0000-0002-8241-6231

Miao Xie − *Institute of Functional Nano and Soft Materials (FUNSOM), Soochow University, Suzhou 215123, China;* orcid.org/0000-0002-9797-1449

William A. Goddard III − *Materials and Process Simulation Center, California Institute of Technology, Pasadena, California 91125, United States;* orcid.org/0000-0003-0097-5716

Complete contact information is available at: https://pubs.acs.org/10.1021/acs.jpclett.1c00279

Notes

The authors declare no competing financial interest.

■ ACKNOWLEDGMENTS

T.C. and M.X. thanks the National Natural Science Foundation of China (Grants 21903058 and 22003044), the Natural Science Foundation of Jiangsu Higher Education Institutions (Grant SBK20190810), the Jiangsu Province High-Level Talents (Grant JNHB-106), and the Priority Academic Program Development of Jiangsu Higher Education Institutions (PAPD) for financial support. H.Y. thanks the China Postdoctoral Science Foundation (Grant 2019M660128) for financial support. This work was partly supported by the Collaborative Innovation Center of Suzhou Nano Science & Technology.

■ REFERENCES

(1) Tarascon, J. M.; Armand, M. Issues and Challenges Facing Rechargeable Lithium Batteries. *Nature* **2001**, *414*, 359−367.

(2) Dunn, B.; Kamath, H.; Tarascon, J.-M. Electrical Energy Storage for the Grid: A Battery of Choices. *Science* **2011**, *334*, 928−935.

(3) Yang, Z.; Zhang, J.; Kintner-Meyer, M. C. W.; Lu, X.; Choi, D.; Lemmon, J. P.; Liu, J. Electrochemical Energy Storage for Green Grid. *Chem. Rev.* **2011**, *111*, 3577.

(4) Goodenough, J. B.; Park, K. S. The Li-Ion Rechargeable Battery: A Perspective. *J. Am. Chem. Soc.* **2013**, *135*, 1167−1176.

(5) Cheng, X. B.; Zhang, R.; Zhao, C. Z.; Zhang, Q. Toward Safe Lithium Metal Anode in Rechargeable Batteries: A Review. *Chem. Rev.* **2017**, *117*, 10403−10473.

(6) Xu, W.; Wang, J.; Ding, F.; Chen, X.; Nasybulin, E.; Zhang, Y.; Zhang, J. G. Lithium Metal Anodes for Rechargeable Batteries. *Energy Environ. Sci.* **2014**, *7*, 513.

(7) Lin, D.; Liu, Y.; Cui, Y. Reviving the Lithium Metal Anode for High-Energy Batteries. *Nat. Nanotechnol.* **2017**, *12*, 194−206.

(8) Zheng, J. M.; Engelhard, M. H.; Mei, D. H.; Jiao, S. H.; Polzin, B. J.; Zhang, J. G.; Xu, W. Electrolyte Additive Enabled Fast Charging and Stable Cycling Lithium Metal Batteries. *Nat. Energy* **2017**, *2*, 17012.

(9) Huang, C.; Xiao, J.; Shao, Y.; Zheng, J.; Bennett, W. D.; Lu, D.; Saraf, L. V.; Engelhard, M.; Ji, L.; Zhang, J.; et al. Manipulating Surface Reactions in Lithium-Sulphur Batteries Using Hybrid Anode Structures. *Nat. Commun.* **2014**, *5*, 3015.

(10) Shi, F.; Pei, A.; Boyle, D. T.; Xie, J.; Yu, X.; Zhang, X.; Cui, Y. Lithium Metal Stripping Beneath the Solid Electrolyte Interphase. *Proc. Natl. Acad. Sci. U. S. A.* **2018**, *115*, 8529−8534.

(11) Scheers, J.; Fantini, S.; Johansson, P. A Review of Electrolytes for Lithium−Sulphur Batteries. *J. Power Sources* **2014**, *255*, 204−218.

(12) Ding, F.; Xu, W.; Chen, X.; Zhang, J.; Engelhard, M. H.; Zhang, Y.; Johnson, B. R.; Crum, J. V.; Blake, T. A.; Liu, X.; et al. Effects of Carbonate Solvents and Lithium Salts on Morphology and Coulombic Efficiency of Lithium Electrode. *J. Electrochem. Soc.* **2013**, *160*, A1894−A1901.

(13) Xu, K. Electrolytes and Interphases in Li-ion Batteries and Beyond. *Chem. Rev.* **2014**, *114*, 11503−11618.

(14) Li, S.; Jiang, M.; Xie, Y.; Xu, H.; Jia, J.; Li, J. Developing High-Performance Lithium Metal Anode in Liquid Electrolytes: Challenges and Progress. *Adv. Mater.* **2018**, *30*, 1706375.

(15) Yamada, Y.; Takazawa, Y.; Miyazaki, K.; Abe, T. Electrochemical Lithium Intercalation into Graphite in Dimethyl Sulfoxide-Based Electrolytes: Effect of Solvation Structure of Lithium Ion. *J. Phys. Chem. C* **2010**, *114*, 11680−11685.

(16) Yoshida, K.; Nakamura, M.; Kazue, Y.; Tachikawa, N.; Tsuzuki, S.; Seki, S.; Dokko, K.; Watanabe, M. Oxidative-Stability Enhancement and Charge Transport Mechanism in Glyme-Lithium Salt Equimolar Complexes. *J. Am. Chem. Soc.* **2011**, *133*, 13121−13129.

(17) Ueno, K.; Yoshida, K.; Tsuchiya, M.; Tachikawa, N.; Dokko, K.; Watanabe, M. Glyme-Lithium Salt Equimolar Molten Mixtures: Concentrated Solutions or Solvate Ionic Liquids? *J. Phys. Chem. B* **2012**, *116*, 11323−11331.

(18) Yamada, Y.; Yaegashi, M.; Abe, T.; Yamada, A. A Super-Concentrated Ether Electrolyte for Fast-Charging Li-Ion Batteries. *Chem. Commun.* **2013**, *49*, 11194−11196.

(19) Zhang, X. Q.; Chen, X.; Cheng, X. B.; Li, B. Q.; Shen, X.; Yan, C.; Huang, J. Q.; Zhang, Q. Highly Stable Lithium Metal Batteries

Enabled by Regulating the Li^+ Solvation in Nonaqueous Electrolyte. *Angew. Chem., Int. Ed.* **2018**, *57*, 5301−5305.
(20) Jie, Y.; Ren, X.; Cao, R.; Cai, W.; Jiao, S. Advanced Liquid Electrolytes for Rechargeable Li Metal Batteries. *Adv. Funct. Mater.* **2020**, *30*, 1910777.
(21) Wang, C.; Fu, K.; Kammampata, S. P.; McOwen, D. W.; Samson, A. J.; Zhang, L.; Hitz, G. T.; Nolan, A. M.; Wachsman, E. D.; Mo, Y.; et al. Garnet-Type Solid-State Electrolytes: Materials, Interfaces, and Batteries. *Chem. Rev.* **2020**, *120*, 4257−4300.
(22) Wu, C.; Guo, F.; Zhuang, L.; Ai, X.; Zhong, F.; Yang, H.; Qian, J. Mesoporous Silica Reinforced Hybrid Polymer Artificial Layer for High-Energy and Long-Cycling Lithium Metal Batteries. *ACS Energy Lett.* **2020**, *5*, 1644−1652.
(23) Cheng, X. B.; Zhang, R.; Zhao, C. Z.; Wei, F.; Zhang, J. G.; Zhang, Q. A Review of Solid Electrolyte Interphases on Lithium Metal Anode. *Adv. Sci.* **2016**, *3*, 1500213.
(24) Markus, I. M.; Jones, G.; Garcia, J. M. Investigation of Electrolyte Concentration Effects on the Performance of Lithium Oxygen Batteries. *J. Phys. Chem. C* **2016**, *120*, 5949−5957.
(25) Suo, L.; Hu, Y.-S.; Li, H.; Armand, M.; Chen, L. A New Class of Solvent-in-Salt Electrolyte for High-Energy Rechargeable Metallic Lithium Batteries. *Nat. Commun.* **2013**, *4*, 1481.
(26) Qian, J. F.; Henderson, W. A.; Xu, W.; Bhattacharya, P.; Engelhard, M.; Borodin, O.; Zhang, J. G. High Rate and Stable Cycling of Lithium Metal Anode. *Nat. Commun.* **2015**, *6*, 6362.
(27) Kim, H.; Wu, F.; Lee, J. T.; Nitta, N.; Lin, H.-T.; Oschatz, M.; Cho, W. I.; Kaskel, S.; Borodin, O.; Yushin, G. In Situ Formation of Protective Coatings on Sulfur Cathodes in Lithium Batteries with LiFSI-Based Organic Electrolytes. *Adv. Energy Mater.* **2015**, *5*, 1401792.
(28) Camacho-Forero, L. E.; Smith, T. W.; Balbuena, P. B. Effects of High and Low Salt Concentration in Electrolytes at Lithium−Metal Anode Surfaces. *J. Phys. Chem. C* **2017**, *121*, 182−194.
(29) Kamphaus, E. P.; Angarita-Gomez, S.; Qin, X.; Shao, M.; Engelhard, M.; Mueller, K. T.; Murugesan, V.; Balbuena, P. B. Role of Inorganic Surface Layer on Solid Electrolyte Interphase Evolution at Li-Metal Anodes. *ACS Appl. Mater. Interfaces* **2019**, *11*, 31467−31476.
(30) Sodeyama, K.; Yamada, Y.; Aikawa, K.; Yamada, A.; Tateyama, Y. Sacrificial Anion Reduction Mechanism for Electrochemical Stability Improvement in Highly Concentrated Li-Salt Electrolyte. *J. Phys. Chem. C* **2014**, *118*, 14091−14097.
(31) Wang, Y.; Liu, Y.; Tu, Y.; Wang, Q. Reductive Decomposition of Solvents and Additives toward Solid Electrolyte Interphase Formation in Lithium-Ion Battery. *J. Phys. Chem. C* **2020**, *124*, 9099−9108.
(32) Wang, A.; Kadam, S.; Li, H.; Shi, S.; Qi, Y. Review on Modeling of the Anode Solid Electrolyte Interphase (SEI) for Lithium-Ion Batteries. *npj Comput. Mater.* **2018**, *4*, 15.
(33) Camacho-Forero, L. E.; Smith, T. W.; Bertolini, S.; Balbuena, P. B. Reactivity at the Lithium−Metal Anode Surface of Lithium−Sulfur Batteries. *J. Phys. Chem. C* **2015**, *119*, 26828−26839.
(34) Bertolini, S.; Balbuena, P. B. Buildup of the Solid Electrolyte Interphase on Lithium-Metal Anodes: Reactive Molecular Dynamics Study. *J. Phys. Chem. C* **2018**, *122*, 10783−10791.
(35) van Duin, A. C. T.; Dasgupta, S.; Lorant, F.; Goddard, W. A. ReaxFF: A Reactive Force Field for Hydrocarbons. *J. Phys. Chem. A* **2001**, *105*, 9396−9409.
(36) Chenoweth, K.; van Duin, A. C. T.; Goddard, W. A. ReaxFF Reactive Force Field for Molecular Dynamics Simulations of Hydrocarbon Oxidation. *J. Phys. Chem. A* **2008**, *112*, 1040−1053.
(37) Bedrov, D.; Smith, G. D.; van Duin, A. C. T. Reactions of Singly-Reduced Ethylene Carbonate in Lithium Battery Electrolytes: A Molecular Dynamics Simulation Study Using the ReaxFF. *J. Phys. Chem. A* **2012**, *116*, 2978−2985.
(38) Islam, M. M.; Bryantsev, V. S.; van Duin, A. C. T. ReaxFF Reactive Force Field Simulations on the Influence of Teflon on Electrolyte Decomposition During Li/SWCNT Anode Discharge in Lithium-Sulfur Batteries. *J. Electrochem. Soc.* **2014**, *161*, E3009−E3014.
(39) Islam, M. M.; Kolesov, G.; Verstraelen, T.; Kaxiras, E.; van Duin, A. C. T. eReaxFF: A Pseudoclassical Treatment of Explicit Electrons within Reactive Force Field Simulations. *J. Chem. Theory Comput.* **2016**, *12*, 3463−3472.
(40) Liu, Y.; Yu, P. P.; Wu, Y.; Yang, H.; Xie, M.; Huai, L. Y.; Goddard, W. A.; Cheng, T. The DFT-ReaxFF Hybrid Reactive Dynamics Method with Application to the Reductive Decomposition Reaction of the TFSI and DOL Electrolyte at a Lithium−Metal Anode Surface. *J. Phys. Chem. Lett.* **2021**, *12*, 1300−1306.
(41) Kresse, G.; Hafner, J. Ab initio Molecular-Dynamics Simulation of the Liquid-Metalamorphous-Semiconductor Transition in Germanium. *Phys. Rev. B: Condens. Matter Mater. Phys.* **1994**, *49*, 14251−14269.
(42) Plimpton, S. Fast Parallel Algorithms for Short-Range Molecular Dynamics. *J. Comput. Phys.* **1995**, *117*, 1−19.
(43) Perdew, J. P.; Burke, K.; Ernzerhof, M. Generalized Gradient Approximation Made Simple. *Phys. Rev. Lett.* **1996**, *77*, 3865−3868.
(44) Naserifar, S.; Oppenheim, J. J.; Yang, H.; Zhou, T.; Zybin, S.; Rizk, M.; Goddard, W. A. Accurate Non-Bonded Potentials Based on Periodic Quantum Mechanics Calculations for Use in Molecular Simulations of Materials and Systems. *J. Chem. Phys.* **2019**, *151*, 154111.
(45) Monkhorst, H. J.; Pack, J. D. Special Points for Brillouin-Zone Integrations. *Phys. Rev. B* **1976**, *13*, 5188−5192.
(46) Kresse, G.; Joubert, D. From Ultrasoft Pseudopotentials to the Projector Augmented-Wave Method. *Phys. Rev. B: Condens. Matter Mater. Phys.* **1999**, *59*, 1758−1775.
(47) Fan, X.; Chen, L.; Ji, X.; Deng, T.; Hou, S.; Chen, J.; Zheng, J.; Wang, F.; Jiang, J.; Xu, K.; Wang, C. Highly Fluorinated Interphases Enable High-Voltage Li-Metal Batteries. *Chem.* **2018**, *4*, 174−185.
(48) Yun, K.-S.; Pai, S. J.; Yeo, B. C.; Lee, K.-R.; Kim, S.-J.; Han, S. S. Simulation Protocol for Prediction of a Solid-Electrolyte Interphase on the Silicon-Based Anodes of a Lithium-Ion Battery: ReaxFF Reactive Force Field. *J. Phys. Chem. Lett.* **2017**, *8*, 2812−2818.
(49) Ospina-Acevedo, F.; Guo, N.; Balbuena, P. B. Lithium Oxidation and Electrolyte Decomposition at Li-Metal/Liquid Electrolyte Interfaces. *J. Mater. Chem. A* **2020**, *8*, 17036−17055.
(50) Köhler, L.; Kresse, G. Density Functional Study of CO on Rh(111). *Phys. Rev. B: Condens. Matter Mater. Phys.* **2004**, *70*, 165405.
(51) Qian, J.; Baskin, A.; Liu, Z.; Prendergast, D.; Crumlin, E. J. Addressing the Sensitivity of Signals from Solid/Liquid Ambient Pressure XPS (APXPS) Measurement. *J. Chem. Phys.* **2020**, *153*, 044709.
(52) Zhang, P.; Zhu, J. J.; Wang, M.; Imanishi, N.; Yamamoto, O. Lithium Dendrite Suppression and Cycling Efficiency of Lithium Anode. *Electrochem. Commun.* **2018**, *87*, 27−30.

https://doi.org/10.1021/acs.jpclett.1c00279
J. Phys. Chem. Lett. 2021, 12, 2922−2929